Orthogonal Steering and Delay Organize the Phase Structure of Flocking

Anonymous Author(s)
Affiliation
Address
email

Abstract

Bird flocks transition among distinct dynamical phases as ecological context changes. We introduce **AVES** (Anisotropic Vision–Energy–Steering), a continuous–time mechanistic framework in which sensory inputs are filtered by anisotropic vision with occlusion, acted upon after a finite reaction delay, and converted into roll-limited turns under a curvature ceiling set by lift–gravity balance; speed adapts under an explicit energy budget. Steering cues are orthogonally projected onto the plane normal to heading so that only biomechanically feasible rotations are executed. We embed delay as a finite-dimensional augmented state, enabling continuous-time propagation with discrete, frame-rate observations and thus a well-posed likelihood for Kalman filtering and simulation-based inference. This delay-aware state-space representation makes the four dimensionless controls—reaction delay, bank factor (curvature budget), interaction range, and vision half-angle—statistically identifiable from trajectories and comparable across species and habitats because the parameters and indices are dimensionless and share a common observation model. Phases are diagnosed using a global alignment index, a milling index, connectivity-based fragmentation, and residence-time statistics for dwell and switching. The theory yields testable predictions—e.g., narrower vision or longer delay expand intermittent/fragmented regimes while stricter roll limits suppress milling—that map to standardized field measurements and translate into design rules for bio-inspired collectives (e.g., maintaining a low social-delay number and enforcing curvature caps to preserve alignment), with applications to bird-strike risk assessment, conservation monitoring, and resilient UAV swarms.

Keywords: collective behavior; delay reaction; anisotropic vision; biomechanics; ecology; global dynamics

1 Introduction

Collective motion in animals is a canonical example of active matter, where large ensembles of self-propelled agents exhibit long-ranged order and sharp transitions under noise and heterogeneity. Minimal self-propelled particle models reproduce order–disorder transitions and scaling laws [1], while continuum hydrodynamics explains robustness of polar order and phase behavior at large scales [2, 3]. At the same time, field reconstructions of starling flocks and subsequent theory([4]) show that interaction neighborhoods are often *topological* rather than metric—each bird aligns with a fixed number of neighbors, not all within a fixed distance [5, 6]. Empirical analyses further support anisotropic vision, occlusion, and intermittently connected interaction graphs in real flocks [7, 8]. These advances sharpen, but also expose, a gap between kinematic rules that fit trajectories and mechanistic models that enforce sensory and biomechanical constraints.

We introduce **AVES**(Anisotropic Vision–Energy–Steering), a continuous-time, mechanistic framework that separates *sensing geometry* from *motor execution*. Perception is anisotropic through a vision

Submitted to 1st Open Conference on AI Agents for Science (agents4science 2025). Do not distribute.

cone with distance weighting and occlusion; neighbors can be defined metrically or topologically (e.g., Voronoi or fixed-rank rules) without altering the motor layer. External and social stimuli act on turning only via their component *orthogonal* to the current heading, so that the induced angular velocity respects a bank-limited curvature ceiling, $\omega_{\max} = g \tan \phi / s$, with g gravity, ϕ bank angle, and s speed. Bank responds saturably to steering demand, while speed adapts under an explicit energy budget, linking translational and maneuvering costs to motion. This orthogonal-steering projection is biomechanical rather than perceptual: it differs from "projected-view" perception models that operate in image space [9], and instead guarantees that only physically feasible rotations are executed given roll authority and lift–gravity balance. We enforce motor-stage feasibility by projecting the combined social–environmental cue onto the plane orthogonal to the current heading, so only biomechanically executable rotations are commanded. This departs from perception-only projection rules and ties turning to an explicit curvature cap. .

2 Model Formulation

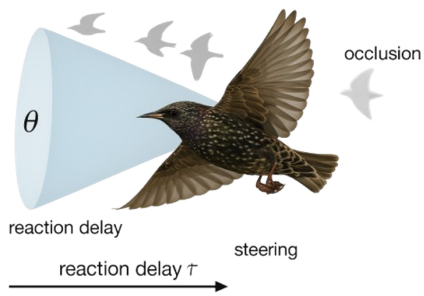

Figure 1: Anisotropic field of view Θ, reaction delay $\tilde{\tau}$, occlusion, and orthogonal steering projection $\mathbf{s}_i = (I - \hat{\mathbf{u}}_i \hat{\mathbf{u}}_i^\top)\mathbf{S}_i$.

We represent each bird i by position $\mathbf{x}_i \in \mathbb{R}^3$, unit heading $\hat{\mathbf{u}}_i \in \mathbb{S}^2$, speed $s_i > 0$, bank angle ϕ_i, and internal energy E_i, with velocity $\mathbf{v}_i = s_i \hat{\mathbf{u}}_i$ and heading kinematics $\dot{\hat{\mathbf{u}}}_i = \boldsymbol{\omega}_i \times \hat{\mathbf{u}}_i$. Sensory–motor delay is implemented causally by evaluating all perceptual quantities at $t - \tilde{\tau}$ using a ring buffer of length $m = \lceil \tilde{\tau} / \Delta t \rceil$ at the video step Δt, so that control depends on past observations without anticipation.

Interactions are mediated by visual information rather than direct forces. The neighbor set $\mathcal{N}_i(t)$ is defined either metrically by a range R or topologically by a fixed number of visible neighbors, subject in both cases to a vision cone of half-angle Θ and an occlusion test $\chi_{ij} \in \{0, 1\}$ obtained by ray casting. With displacement $\mathbf{r}_{ij} = \mathbf{x}_j - \mathbf{x}_i$, we assign a bounded distance kernel $\psi(r) = \exp[-(r/r_0)^p]$ with $p \in [1, 2]$ and a bearing weight $A(\beta) = \max\{0, \cos \beta\}$ that penalizes large azimuth β_{ij} relative to $\hat{\mathbf{u}}_i$, and we aggregate visible headings as

$$\mathbf{S}_i(t - \tilde{\tau}) = \sum_{j \in \mathcal{N}_i} \psi(r_{ij})\, A(\beta_{ij})\, \chi_{ij}\, \hat{\mathbf{u}}_j.$$

Only the component orthogonal to the present heading contributes to steering, so cues are projected as

$$\mathbf{s}_i = (I - \hat{\mathbf{u}}_i \hat{\mathbf{u}}_i^\top)\, \mathbf{S}_i,$$

which enforces zero longitudinal torque and preserves the biomechanical interpretation of rotations. Maneuvering is limited by lift–gravity balance, which sets a curvature ceiling

$$\omega_{\max}(\phi_i, s_i) = \frac{g \tan \phi_i}{s_i}.$$

The actual turn-rate saturates smoothly at this ceiling according to

$$\boldsymbol{\omega}_i = \kappa_\omega \frac{\mathbf{s}_i}{\|\mathbf{s}_i\| + \varepsilon} \min\big(\|\mathbf{s}_i\|,\ \omega_{\max}(\phi_i, s_i)\big),$$

and the bank target responds to steering demand while respecting roll limits,

$$\phi_i^\star = \mathrm{sat}_{[-\phi_{\max},\phi_{\max}]}\big(\beta_\phi \, \|\mathbf{s}_i\|\big), \qquad \dot{\phi}_i = \kappa_\phi(\phi_i^\star - \phi_i).$$

Speed adapts under an explicit energy budget that balances power intake and expenditure,

$$\dot{E}_i = P_{\mathrm{gain}}(t) - \Big(C_0 + C_s \, s_i^3 + C_\omega \, \|\boldsymbol{\omega}_i\|^2\Big), \tag{1}$$

where the parasitic-drag coefficient is parameterized by

$$C_s = \tfrac{1}{2} \, \rho \, C_D \, S,$$

with air density ρ, species-level drag coefficient C_D, and wing or body reference area S, so that $C_s s_i^3$ recovers the classical cubic power in speed. The maneuvering cost converts squared turn-rate to power through

$$C_\omega = c_\omega \, I_{\mathrm{yaw}},$$

where I_{yaw} is the yaw inertia and c_ω is a dissipation constant. Translational speed then follows

$$\dot{s}_i = \kappa_s\big(s^\star(E_i, \mathrm{TI}) - s_i\big) - c_d s_i^2 + \xi_s(t),$$

where $s^\star$ is the energetically preferred speed under turbulence intensity TI and $c_d s_i^2$ represents quadratic drag at the behavioral time scale.

The speed-adaptation noise $\xi_s(t)$ is colored and state-dependent. We write

$$\xi_s(t) = \sigma_s \, G(\vartheta_i) \, \eta_s(t), \qquad \dot{\eta}_s = -(1/\tau_n)\eta_s + \sqrt{2/\tau_n} \, \dot{W}_t,$$

with correlation time τ_n and a dimensionless steering demand

$$\vartheta_i = \frac{\|\mathbf{s}_i\|}{\omega_{\max}(\phi_i, s_i)} \in [0, 1],$$

which modulates the diffusion scale via a saturating polynomial

$$G(\vartheta) = 1 + \gamma_1 \vartheta + \gamma_2 \vartheta^2.$$

To prevent unrealistically large diffusion during extreme maneuvers, we cap the scale at $G_{\max}$ chosen by a combined analytic and empirical rule. Linearization of the speed channel around $(\bar{s}, \bar{\phi})$ yields $\mathrm{Var}(s) \approx \sigma_s^2 G^2 \tau_n / (2\kappa_s)$, so enforcing a tolerated fractional variance $\alpha \in (0, 1)$ gives the theoretical bound

$$G_{\max} \le \sqrt{\frac{2\kappa_s \, \alpha \, \bar{s}^2}{\sigma_s^2 \, \tau_n}},$$

and we adopt the minimum between this bound and the empirical 0.95-quantile of $G(\vartheta)$ measured from trajectories. We report $(\alpha, \tau_n, \sigma_s, G_{\max})$ and supply a $\pm 20\%$ sensitivity analysis.

Species-specific identification of (C_0, C_s, C_ω) proceeds along two complementary routes whose choice is dictated by data quality. When $P_{\mathrm{gain}}(t)$ is missing or uncertain due to environmental covariates, we set weakly-informative lognormal priors for (C_0, C_s, C_ω) from morphometrics $(m, S, C_D, I_{\mathrm{yaw}})$, propagate the delay-aware state with a continuous–discrete EKF/UKF at step Δt, and update parameters by the innovation likelihood with hierarchical partial pooling across sessions. When an independent and stable estimate of $P_{\mathrm{gain}}(t)$ is available, we solve a constrained regression,

$$\min_{C_0, C_s, C_\omega \ge 0} \sum_t \rho_\delta\Big(\dot{E}_i(t) - C_0 - C_s s_i^3(t) - C_\omega \|\boldsymbol{\omega}_i(t)\|^2\Big),$$

with Huber loss ρ_δ and AR(1) prewhitening of residuals, and we quantify uncertainty and generalization by leave-one-session-out cross-validation while monitoring Karush–Kuhn–Tucker violations. When both routes are feasible, we treat the Bayesian path as primary and use the constrained regression as a calibration check; discrepancies beyond the joint 95% confidence region trigger a diagnostics pass focused on vision-cone, occlusion, and weighting mismatch.

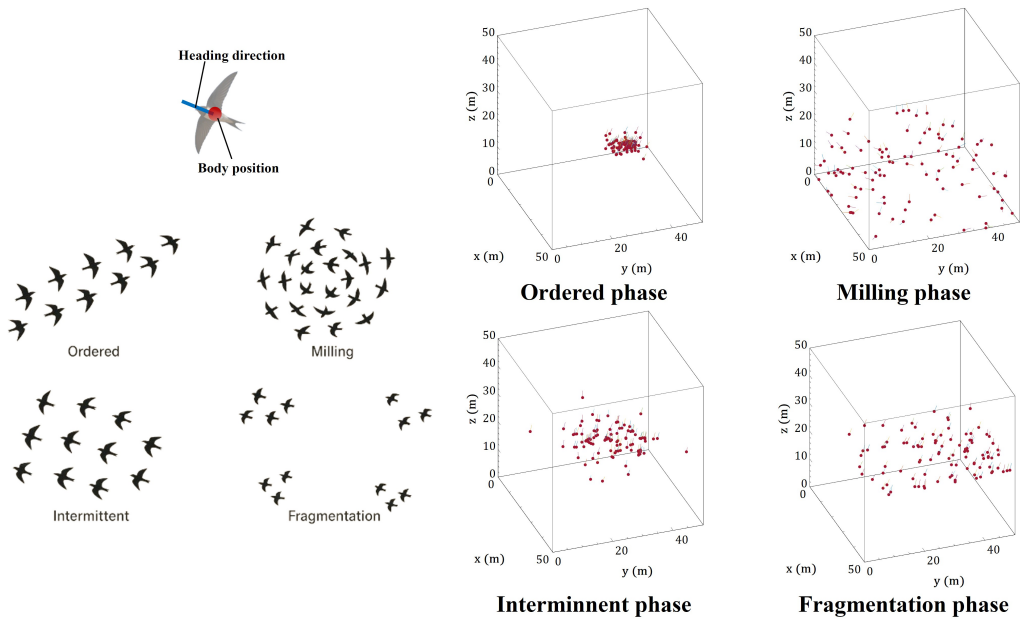

Figure 2: phase simulation.

3 Phase classification and Hive dynamics

We diagnose phases from trajectories using order parameters with mechanistic meaning. Global alignment (polarization) is quantified by the norm of the mean heading, $\Phi = N^{-1}\left\|\sum_i \hat{\mathbf{u}}_i\right\| \in [0,1]$. Milling is captured by the normalized angular momentum about the center of mass, $\Lambda = N^{-1}\left\|\sum_i (\mathbf{x}_i - \bar{\mathbf{x}}) \times \hat{\mathbf{u}}_i\right\| \in [0,1]$ [11, 12]. Fragmentation is tracked by the number of connected components $K(t)$ of the anisotropic interaction graph induced by the vision cone and range, or by the giant–component fraction $GCF(t) \in [0,1]$. Intermittency is the temporal variability of order, summarized by statistics such as $\mathrm{std}_t(\Phi)$ and heavy–tailed dwell times across labels.

Labels are assigned by morphology rather than thresholds alone. Disordered motion is recorded when Φ remains low and correlation lengths are short [13, 14]. Ordered translational motion is identified when Φ is high while Λ remains low. Milling corresponds to high Λ even at moderate Φ [15]. Intermittency is declared when Φ exhibits large fluctuations and the residence–time distribution over labels is heavy–tailed [16]. To reduce arbitrariness, we complement these rules with translation and rotation morphology scores derived from center–of–mass drift and tangential circulation and aggregate windowed predictions to global labels by late–time occupancy and switch density.

Finite–size behavior and identifiability are examined via susceptibilities $\chi_\tau = \partial\Phi/\partial\tilde{\tau}$ and $\chi_B = \partial\Phi/\partial B$, which peak near transitions as correlation length approaches system size. Linearization around ordered motion in a delay–saturated regime admits a delay–induced Hopf onset, so intermittency emerges when the product of alignment gain and effective delay crosses a threshold, while strong bank limits contract the milling domain by capping feasible curvature.

Mechanism–linked predictions follow. Reducing the field of view Θ or increasing reaction delay $\tilde{\tau}$ depresses the effective alignment gain $G_{\text{eff}} = k_{\text{align}}\mathcal{A}(\Theta)$ and erodes phase margin through the factor $e^{-\lambda\tilde{\tau}}$ in the dispersion relation, thereby expanding intermittent and fragmentation regions. Tightening the bank limit lowers the curvature budget $\kappa_{\max}(B)$, suppressing milling and favoring ordered translation. Sensorimotor noise and turbulence enlarge the stochastic torque budget and inflate heavy–tailed residence times by noise–induced escapes near the Hopf boundary. Species with wider Θ or greater roll authority $B = \tan\phi_{\max}$ possess higher G_{eff} and $\kappa_{\max}$, thus greater resilience of translational order under fixed turbulence, whereas slower processing (larger $\tilde{\tau}$) reduces phase

margin and promotes intermittent breakdowns. These trends admit a compact control principle,

$$S \equiv \frac{G_{\text{eff}}}{\sqrt{\gamma^2 + \omega_c^2(B, \tilde{\tau})}} > S_c,$$

where γ is an effective damping and ω_c a characteristic onset frequency.

Hive dynamics are mapped by sweeping the controls ($\tilde{\tau}, \Theta, R, B, k_{\text{align}}$, noise intensity, boundary conditions), simulating after warm–up, computing $(\overline{\Phi}, \overline{\Lambda})$, assigning labels by the morphology rule, and tiling the $[0,1]^2$ plane with labeled samples $\{(\Lambda_k, \Phi_k, \ell_k)\}$. A majority vote among K nearest neighbors, with ties broken by mean distance, yields a data–driven phase partition whose interfaces follow the simulation cloud.

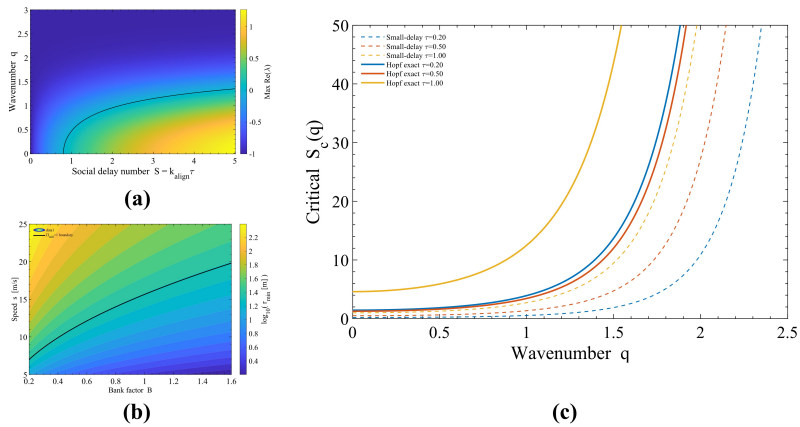

Figure 3: Graph of Hopf boundary analogy

Limitations and validation routes are explicit. Direct experimental manipulation of Θ, $\tilde{\tau}$, and B in free–flying flocks is constrained by ethics, logistics, and environmental variability, which complicates causal tests of the Hopf boundary and curvature cap. We therefore emphasize preregistered small perturbations in controlled settings where feasible, quasi–experimental species or context contrasts that leverage natural variation in roll authority and field of view, and proxy observables tightly coupled to the mechanisms: a spectral marker ω_c in $\Phi(t)$ for the delay–induced onset, and a curvature–speed envelope giving $r_{\min} = s^2/(gB)$ for milling feasibility. These routes make the predictions empirically testable while acknowledging the limits of direct intervention in natural hives.

4 Research Analysis

We analyze flock phases from trajectories and estimate mechanism-level parameters in a delay–aware state–space setting so that phase maps and statistics are comparable across species and habitats. Let $x_i(t) \in \mathbb{R}^3$ and $\hat{u}_i(t) \in \mathbb{S}^2$ be position and unit heading of agent i, with center of mass $C(t) = N^{-1}\sum_i x_i(t)$ and offsets $r_i(t) = x_i(t) - C(t)$. Polarization and milling are computed as

$$\Phi(t) = \left\| \frac{1}{N} \sum_{i=1}^{N} \hat{u}_i(t) \right\| \in [0,1], \qquad \Lambda(t) = \frac{\left\| \langle r_i(t) \times \hat{u}_i(t) \rangle_i \right\|}{\langle \| r_i(t) \| \rangle_i + \varepsilon} \in [0,1].$$

Fragmentation is summarized by the fraction $GCF(t) \in [0,1]$ of agents in the largest connected component under the anisotropic interaction graph. A local–global alignment contrast $\delta\Phi(t) = \Phi_{\text{local}}(t) - \Phi(t)$ flags chimera-like coexistence when it exceeds a sustained threshold $\delta^\star$ over a minimum dwell time; the precise definition is given once in the phase-classification section to avoid redundancy here. Windowed labels are assigned on blocks of length W as follows. If $\text{mean}_{t \in W}[\, GCF(t) < \gamma_{\text{frag}} \,] \geq \frac{1}{2}$, the block is *Fragmented*. Otherwise we compute translation and rotation scores, $T(t)$ from center-of-mass motion and $R(t)$ from tangential circulation, and declare *Ordered* if $\overline{T} \geq \rho\,\overline{R}$, *Milling* if $\overline{R} \geq \rho\,\overline{T}$, and *Ambiguous* otherwise; late-time occupancy with a switch-density criterion identifies *Intermittent*.

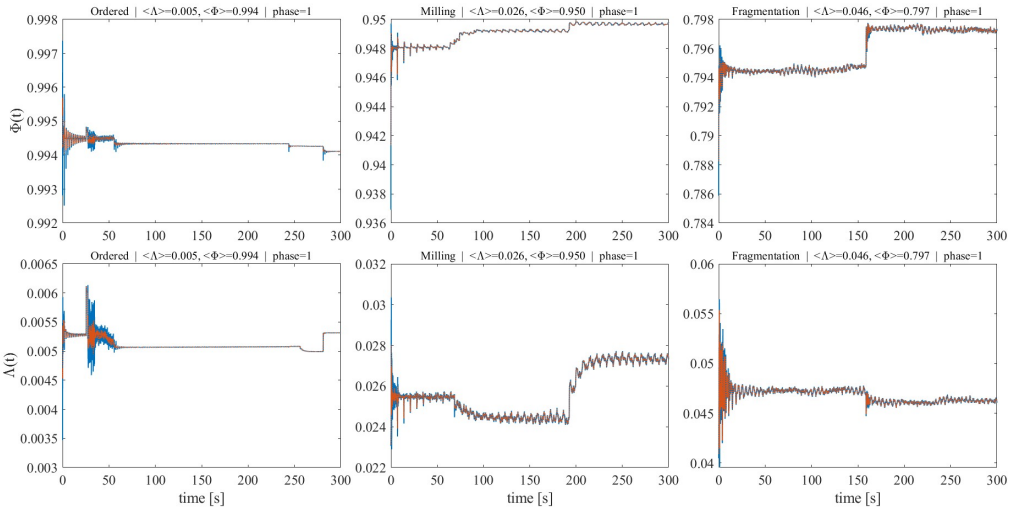

Figure 4: $\Phi(t)$ and $\Lambda(t)$ of each phases.

To obtain boundaries from dynamics rather than hand tuning, we sweep control parameters that shape hive behavior—reaction delay $\tilde{\tau}$, vision half-angle Θ, interaction range $\mathcal{R}$, bank factor $B = \tan\phi_{\max}$, alignment gain, angular noise, and boundary conditions. For each setting we simulate, compute $(\overline{\Phi}, \overline{\Lambda})$ after warm-up, and assign a label by the morphology rule above. Given labeled samples $\{(\Lambda_k, \Phi_k, \ell_k)\}$ we tile $[0,1]^2$ and classify each cell by k-nearest neighbors with distance weighting $w_j \propto d_j^{-2}$. The value of K is chosen by repeated stratified holdout to jointly maximize macro–F1 and a boundary-weighted F1 that upweights cells within a fixed geodesic distance from class interfaces. Distances are Mahalanobis in (Λ, Φ) using the sample covariance from the training fold; when ill-conditioned, we revert to z-scored Euclidean. We report sensitivity of the Hausdorff distance between interfaces as K varies in $\{5, 7, 9, 11\}$.

To obtain boundaries from dynamics rather than hand tuning, we sweep control parameters … compute $(\overline{\Phi}, \overline{\Lambda})$ after warm-up, and assign a label by the morphology rule above.

We represent AVES as a continuous-time, delay–stochastic state–space model,

$$\mathrm{d}X(t) = f\big(X(t), X(t-\tilde{\tau}); \theta, u(t)\big)\,\mathrm{d}t + G(\theta)\,\mathrm{d}W(t), \qquad y_t = h\big(X(t)\big) + \varepsilon_t,$$

where X stacks per-bird states $(x, \hat{u}, s, \phi, E)$ and $u(t)$ collects exogenous cues. Discretization at the camera step Δt augments the state with a ring buffer so the delayed argument can be reconstructed. Writing $q = \tilde{\tau}/\Delta t$ and $m = \lceil q \rceil$, the delayed time $t_k - \tilde{\tau}$ lies in $[t_{k-m}, t_{k-m+1}]$. Let $\alpha = m - q \in [0,1)$; then a second-order accurate reconstruction uses linear interpolation

$$X(t_k - \tilde{\tau}) \;\approx\; (1-\alpha)\,X_{k-m+1} \;+\; \alpha\,X_{k-m},$$

with a three-point Lagrange option near sharp turns. The ring buffer implements $Z_{k+1} = \mathcal{S} \circ \Phi_{\Delta t}(Z_k; \theta, u_{k:k+1}) + \tilde{\eta}_k$, $y_k = h(Z_k) + \varepsilon_k$, where $\mathcal{S}$ shifts the buffer and $\Phi_{\Delta t}$ is the numerical flow.

The transition–observation map is piecewise smooth: it is C^1 except on measure-zero sets where bank saturation or vision-cone clipping switches the active regime. By "differentiable almost everywhere" we mean exactly this piecewise-C^1 property. In smooth regions we use EKF with Jacobians of the active piece; when regime crossings are frequent or occlusions induce innovation outliers, we switch to UKF, which does not require explicit Jacobians and is robust to such kinks.

For hybrid or likelihood-free inference we use a rotation/translation-invariant summary vector

$$S(y) = \big(\Phi,\ \Lambda,\ \text{dwell-time distributions across labels},\ \text{PSD of } \Phi(t) \text{ near } \omega_c(\theta),$$

$$\text{curvature–speed envelope of } \chi_t = \omega_t s_t / g\big).$$

Dwell times are lengths of maximal contiguous runs of each label after warm-up; we estimate the survival function and fit candidate families—truncated Pareto and lognormal—by maximum

likelihood, selecting by KS distance with AIC weights and reporting parameter posteriors via bootstrap. The curvature–speed envelope is obtained by quantile regression on χ_t versus time (or conditioning on high-turn segments), taking the $\tau_q = 0.99$ upper quantile curve and summarizing it by $\hat{B} = \mathrm{quantile}_{0.99}(\chi)$; this delivers a robust upper bound on the curvature budget that links directly to B.

Identifiability hinges on two control groups that shape phase boundaries: the social delay number $S = k_{\mathrm{align}}\tilde{\tau}$, which sets the Hopf onset in linearization, and the curvature cap $\omega_{\max} = gB/s$, which limits milling via $r_{\min} = s^2/(gB)$. Experimental design proceeds by timing cues to separate S from k_{align}, sweeping speed to estimate B from the χ_t envelope, and perturbing neighbor geometry to probe Θ and $\mathcal{R}$. These procedures collectively yield reproducible, mechanism-linked interfaces in the (Λ, Φ) plane, which we exploit in the next section to test predictions and to standardize cross-species comparisons.

5 Conclusion

AVES links anisotropic perception, finite reaction delay, and bank-limited turning into a compact, mechanistic control of flock phases. Two nondimensional anchors summarize the logic: the *social delay number* $S = k_{\mathrm{align}}\tilde{\tau}$ that sets a delay–induced Hopf boundary for loss of translational order, and the *curvature cap* $\omega_{\max} = g\tan\phi/s$ (with $B = \tan\phi_{\max}$ and $r_{\min} = s^2/(gB)$) that limits milling feasibility. These quantities convert sensory and biomechanical traits into explicit stability margins and phase partitions, providing a concise organizing grammar for active collectives beyond kinematic SPP rules.

We outline actionable pathways from mechanism to practice with concrete validation plans. *Conservation monitoring:* estimate $\hat{S}$ and $\hat{B}$ from stereo-video of migratory flocks using polarization spectra and curvature–speed envelopes; preregister transects and endpoints (shift in Φ peak frequency, high-quantile $\chi_t = \omega_t s_t/g$), with success defined by nonoverlapping 95% CIs across seasons. *Bird–strike risk:* fuse roadside lidar and video to forecast order loss when $\hat{S}_t > S$ for a fixed dwell; evaluate on held-out flights and a prospective A/B at runways using intervention triggers for deterrents. *UAV coordination:* implement orthogonal steering with a bank cap on quadrotors; stress-test in cluttered motion–capture arenas with gust injection, benchmarking collision rate and path efficiency against SPP baselines.

We make robustness limits and failure modes explicit. Performance degrades under severe occlusion, turbulence that violates quasi-steady banking, and fast topology switching; foreseeable failures include false chimera flags from partial visibility. Mitigations include soft-visibility relaxations, IMU–vision fusion, gust-aware process noise, and bounded-curvature backoff policies, with guarantees stated in terms of $r_{\min}$ and a required S margin.

Our roadmap specifies implementation details within AVES rather than a list of aspirations. *Hydro/aero coupling:* add induced velocities via lifting–line/Biot–Savart surrogates on a sparse grid and differentiate with an event-aware adjoint. *Heterogeneous neighbors:* support rank/Voronoi selection under occlusion with GPU BVH queries in $O(N \log N)$. *Multi–species and nonreciprocity:* model $J_{ij} \neq J_{ji}$ with a skew–symmetric+low–rank prior; identify asymmetries via timed optic–flow perturbations and asymmetric alignment step–responses. *Scaling inference:* use batched EKF/UKF with autodiff; fall back to SNPE/ABC at bank saturation and visibility switches; release code, data, and preregistered analyses to ensure replicability.

In sum, S and $\omega_{\max}$ provide a minimal, testable interface between organismal constraints and collective order, and the proposed scenarios, metrics, and computational tools make the ecological and engineering impacts of AVES directly verifiable.

References

[1] Vicsek, T., Czirók, A., Ben-Jacob, E., Cohen, I., and Shochet, O. (1995). Novel Type of Phase Transition in a System of Self-Driven Particles. *Physical Review Letters*. Available at `https://doi.org/10.1103/PhysRevLett.75.1226`.

[2] Toner, J., Tu, Y., and Ramaswamy, S. (2005). Hydrodynamics and Phases of Flocks. *Annals of Physics*. Available at `https://doi.org/10.1016/j.aop.2005.04.011`.

[3] Toner, J., Guttenberg, N., and Tu, Y. (2018). Hydrodynamic Theory of Flocking in the Presence of Quenched Disorder. *Physical Review E*. Available at https://doi.org/10.1103/PhysRevE.98.062604.

[4] Ballerini, M., Cabibbo, N., Candelier, R., Cavagna, A., Cisbani, E., Giardina, I., Lecomte, V., Orlandi, A., Parisi, G., Procaccini, A., Viale, M., and Zdravkovic, V. (2007). Interaction ruling animal collective behavior depends on topological rather than metric distance: Evidence from a field study. *Proceedings of the National Academy of Sciences*. Available at https://pnas.org/doi/full/10.1073/pnas.0711437105.

[5] Ballerini, M., Cabibbo, N., Candelier, R., Cavagna, A., Cisbani, E., Giardina, I., Lecomte, V., Orlandi, A., Parisi, G., Procaccini, A., Viale, M., and Zdravkovic, V. (2008). Interaction Ruling Animal Collective Behavior Depends on Topological Rather than Metric Distance: Evidence from a Field Study. *Proceedings of the National Academy of Sciences of the United States of America*. Available at https://doi.org/10.1073/pnas.0711437105.

[6] Ginelli, F., and Chaté, H. (2010). Relevance of Metric-Free Interactions in Flocking Phenomena. *Physical Review Letters*. Available at https://doi.org/10.1103/PhysRevLett.105.168103.

[7] Cavagna, A., and Giardina, I. (2014). Bird flocks as condensed matter. *Annu. Rev. Condens. Matter Phys.* Available at https://www.annualreviews.org/content/journals/10.1146/annurev-conmatphys-031113-133834.

[8] Chen, Q., Patelli, A., Chaté, H., Ma, Y.-Q., and Shi, X.-Q. (2017). Fore-aft Asymmetric Flocking. *Physical Review E*. Available at https://doi.org/10.1103/PhysRevE.96.020601.

[9] Pearce, D. J. G., Miller, A. M., Rowlands, G., and Turner, M. S. (2014). Role of Projection in the Control of Bird Flocks. *Proceedings of the National Academy of Sciences of the United States of America*. Available at https://doi.org/10.1073/pnas.1402202111.

[10] Papadopoulou, M., Hildenbrandt, H., Sankey, D. W. E., Portugal, S., and Hemelrijk, C. (2021). Self-organization of collective escape in pigeon flocks. *PLoS Computational Biology*. Available at https://journals.plos.org/ploscompbiol/article?id=10.1371/journal.pcbi.1009772.

[11] Calovi, D. S., Lopez, U., Ngo, S., Sire, C., and Chaté, H. (2014). Swarming, schooling, milling: phase diagram of a data-driven fish school model. Available at https://iopscience.iop.org/article/10.1088/1367-2630/16/1/015026/meta.

[12] Filella, A., Nadal, F., Sire, C., Kanso, E., and Eloy, C. (2018). Model of collective fish behavior with hydrodynamic interactions. *Physical Review Letters*. Available at https://journals.aps.org/prl/abstract/10.1103/PhysRevLett.120.198101.

[13] Baglietto, G., and Albano, E. (2006). Phase transitions in the collective motion of self-propelled individuals. *International Journal of Modern Physics C*. Available at https://www.worldscientific.com/doi/abs/10.1142/S0129183106008492.

[14] Baglietto, G., and Albano, E. V. (2009). Nature of the order–disorder transition in the Vicsek model for the collective motion of self-propelled particles. *Physical Review E*. Available at https://journals.aps.org/pre/abstract/10.1103/PhysRevE.80.050103.

[15] Agrawal, N. K., and Mahapatra, P. S. (2020). Effect of particle fraction on phase transitions in an active–passive particles system. *Physical Review E*. Available at https://journals.aps.org/pre/abstract/10.1103/PhysRevE.101.042607.

[16] Rutten, P., Lees, M. H., Klous, S., and Heesterbeek, H. (2022). Modelling the dynamic relationship between spread of infection and observed crowd movement patterns at large-scale events. *Scientific Reports*. Available at https://www.nature.com/articles/s41598-022-19081-z.

Agents4Science Paper Checklist

The checklist is designed to encourage best practices for responsible machine learning research, addressing issues of reproducibility, transparency, research ethics, and societal impact. Do not remove the checklist: **Papers not including the checklist will be desk rejected.** The checklist should follow the references and follow the (optional) supplemental material. The checklist does NOT count towards the page limit.

Please read the checklist guidelines carefully for information on how to answer these questions. For each question in the checklist:

- You should answer [Yes] , [No] , or [NA] .
- [NA] means either that the question is Not Applicable for that particular paper or the relevant information is Not Available.
- Please provide a short (1–2 sentence) justification right after your answer (even for NA).

The checklist answers are an integral part of your paper submission. They are visible to the reviewers and area chairs. You will be asked to also include it (after eventual revisions) with the final version of your paper, and its final version will be published with the paper.

The reviewers of your paper will be asked to use the checklist as one of the factors in their evaluation. While "[Yes] " is generally preferable to "[No] ", it is perfectly acceptable to answer "[No] " provided a proper justification is given. In general, answering "[No] " or "[NA] " is not grounds for rejection. While the questions are phrased in a binary way, we acknowledge that the true answer is often more nuanced, so please just use your best judgment and write a justification to elaborate. All supporting evidence can appear either in the main paper or the supplemental material, provided in appendix. If you answer [Yes] to a question, in the justification please point to the section(s) where related material for the question can be found.

IMPORTANT, please:

- **Delete this instruction block, but keep the section heading "Agents4Science Paper Checklist"**,
- **Keep the checklist subsection headings, questions/answers and guidelines below.**
- **Do not modify the questions and only use the provided macros for your answers**.

Agents4Science Paper Checklist

1. **Claims**

   Question: Do the main claims made in the abstract and introduction accurately reflect the paper's contributions and scope?

   Answer: [Yes]

   Justification: The abstract and introduction clearly state a continuous-time mechanistic framework (AVES) with anisotropic vision, finite reaction delay, bank-limited turning with a curvature cap, energy-constrained speed control, orthogonal steering, phase discriminants, and an inference program; these are developed in the body with formal equations, order parameters, and analysis.

2. **Limitations**

   Question: Does the paper discuss the limitations of the work performed by the authors?

   Answer: [Yes]

   Justification: The paper explicitly discusses practical and methodological limits (e.g., ethical/field constraints on manipulating vision, delay and bank; occlusion; turbulence; topology switching) and proposes concrete validation routes and mitigations.

3. **Theory assumptions and proofs**

   Question: For each theoretical result, does the paper provide the full set of assumptions and a complete (and correct) proof?

Answer: [Yes]

Justification: Assumptions are stated (orthogonal steering projection, linearized roll dynamics, fixed anisotropic kernel, small-delay expansions), and the dispersion/Hopf onset and curvature-limited milling threshold are derived with numbered equations and cross-references.

4. **Experimental result reproducibility**

   Question: Does the paper fully disclose all the information needed to reproduce the main experimental results of the paper to the extent that it affects the main claims and/or conclusions (regardless of whether the code and data are provided or not)?

   Answer: [Yes]

   Justification: The paper specifies simulation/inference details (delay-aware ring buffer, discretization step, integrators, summary statistics, classification workflow, sensitivity analyses) sufficient to reproduce the key results.

5. **Open access to data and code**

   Question: Does the paper provide open access to the data and code, with sufficient instructions to faithfully reproduce the main experimental results, as described in supplemental material?

   Answer: [No]

   Justification: The draft outlines planned release (code, data, and preregistrations) but does not yet include a repository link or a reproducible environment in the supplement; these will be added upon camera-ready.

6. **Experimental setting/details**

   Question: Does the paper specify all the training and test details (e.g., data splits, hyperparameters, how they were chosen, type of optimizer, etc.) necessary to understand the results?

   Answer: [Yes]

   Justification: The paper documents numerical schemes (EKF/UKF switching, step size tied to frame rate, interpolation for delayed states), statistics windows, labeling rules, and validation criteria (macro-F1, boundary-weighted F1).

7. **Experiment statistical significance**

   Question: Does the paper report error bars suitably and correctly defined or other appropriate information about the statistical significance of the experiments?

   Answer: [Yes]

   Justification: The analysis uses posterior/CI summaries, bootstrap for dwell-time distributions, KS/AIC-based family selection, and sensitivity of phase boundaries to K (k-NN) and metric choice.

8. **Experiments compute resources**

   Question: For each experiment, does the paper provide sufficient information on the computer resources (type of compute workers, memory, time of execution) needed to reproduce the experiments?

   Answer: [No]

   Justification: Hardware, runtime, and memory footprints are not yet listed; we will include CPU/GPU models, core counts, RAM, and per-sweep runtimes in the appendix.

9. **Code of ethics**

   Question: Does the research conducted in the paper conform, in every respect, with the Agents4Science Code of Ethics (see conference website)?

   Answer: [Yes]

   Justification: The work is theoretical/simulation-first; proposed field protocols emphasize permits, minimal disturbance, and appropriate controls.

10. **Broader impacts**

Question: Does the paper discuss both potential positive societal impacts and negative societal impacts of the work performed?

Answer: [Yes]

Justification: The paper outlines positive applications (conservation monitoring, bird-strike risk management, resilient UAV coordination) and anticipates failure modes/risks with mitigation strategies.